Quantum magneto-optics of graphite family

L.A. Falkovsky

Landau Institute for Theoretical Physics, Moscow 119334

Verechagin Institute of the High Pressure Physics, Troitsk 142190

(Dated: March 4, 2013)

Abstract

The optical conductivity of graphene, bilayer graphene, and graphite in quantizing magnetic fields is studied. Both dynamical conductivities, longitudinal and Hall's, are analytically evaluated. The conductivity peaks are explained in terms of electron transitions. We have shown that trigonal warping can be considered within the perturbation theory for strong magnetic fields larger than 1 T and in the semiclassical approach for weak fields when the Fermi energy is much larger than the cyclotron frequency. The main optical transitions obey the selection rule with $\Delta n = 1$ for the Landau number n, however the $\Delta n = 2$ transitions due to the trigonal warping are also possible. The Faraday/Kerr rotation and light transmission/reflection in the quantizing magnetic fields are calculated. Parameters of the Slonczewski–Weiss–McClure model are used in the fit taking into account the previous dHvA measurements and correcting some of them for the case of strong magnetic fields.

I. INTRODUCTION

Comprehensive literature on the graphene family can be described in terms of the Dirac gapless fermions. According to this picture, there are two bands at the K hexagon vertexes of the Brillouin zone without any gap between them, and the electron dispersion can be considered as linear in the wide wave-vector region. For the dispersion linearity, this region should be small compared with the size of the Brillouin zone, i.e. less than 10^{-8} cm^{-1}, providing the small carrier concentration $n \ll 10^{16}$ cm^{-1}. Pristine graphene at zero temperature has no carriers, and the Fermi level should divide the conduction and valence bands. However, undoped graphene cannot be really obtained, and so far purest graphene contains about $n \sim 10^9$ cm^{-2} of carriers. Then the following problem appears — how do Coulomb electron-electron interactions renormalize the linear dispersion and does graphene become an insulator with a gap?

Semiconductors with the gap are needed for electronic applications. Investigations of the graphene bilayer and multilayer are very popular as the gap appears when the bias is applied. We see how physics made a circle for the half of century returning to graphite studies. Here Slonczewski, Weiss, and McClure (SWMC) should be mentioned because they have stated the description of a layered matter[1] with interactions strong in the layer and weak between layers.

The most accurate investigation of the band structure of metals and semiconductors is a study of the Landau levels through experiments such as magneto-optics[2–10] and magneto-transport[11–15]. In magnetic fields, the classical and quantum Hall effects are observed, as well as the polarization rotation for transmitted (the Faraday rotation) or reflected lights (the Kerr rotation). However, the interpretation of the experimental results involves a significant degree of uncertainty, because it is not clear how the resonances can be identified and which electron transitions they correspond to.

The theoretical solution for the band problem in magnetic fields often cannot be exactly found. A typical example is presented by graphene layers. For bilayer graphene and graphite, the effective Hamiltonian is a 4×4 matrix giving four energy bands. Fig. 1 shows the nearest two bands of the level structure together with the semiclassical orbits. The trigonal warping described by the effective Hamiltonian with a relatively small parameter γ_3 provides an evident effect (see the right panel). Another important parameter is the gate-tunable
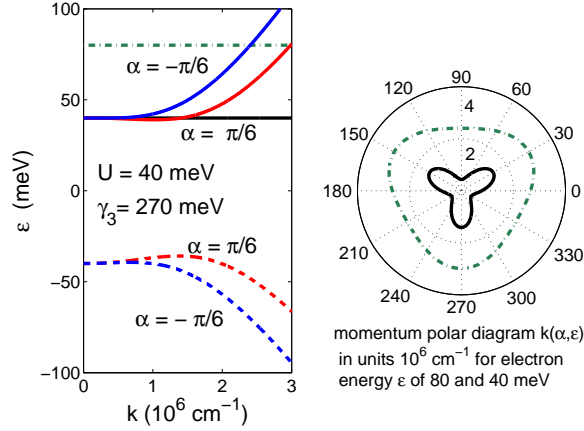
Figure 1: (Color online) (a) The energy dispersion $\varepsilon(k, \alpha)$ of two nearest bands (the electron band shown in solid line and the hole band in dashed line) in bilayer graphene for two polar angles α with the local extrema at $k \neq 0$ ("mexican hat") represented. The band parameters are given in the figure, others are $\gamma_0 = 3.05$ eV, $\gamma_1 = 360$ meV, $\gamma_4 = -150$ meV. (b) Cross-sections $k(\alpha, \varepsilon)$ of the electron band for energies of 80 meV (dashed-dotted line) and 40 meV (solid line).

bandgap U in bilayer graphene. In this situation, the quantization problem cannot be solved within a rigorous method. To overcome this difficulty several methods have been proposed for approximate[9,16–19], numerical[20–24], and semiclassical quantization[25,26].

The present paper is organized as follows. In Sec. II we recall the electron dispersion in the graphene, bilayer graphene, and graphite. In Sec. III the optical conductivity and light transmission are discussed. In Secs. IV and V we describe in detail the quantization in magnetic fields. In Sec. VI the longitudinal and Hall conductivities as well as the Faraday/Kerr rotation are described.

II. ELECTRON DISPERSION IN GRAPHENE FAMILY

A. Electron dispersion in graphene

The symmetry of K point is C_{3v} with the threefold axis and reflection planes. This group has twofold representation with the basis functions transforming each in other under reflections and obtaining the factors $\exp(\pm 2\pi i/3)$ in rotations. The linear momentum variations from the K point $p_\pm = \mp i p_x - p_y$ transform in a similar way. The effective Hamiltonian is

3

invariant under the group transformations, and we have the unique possibility to construct the invariant Hamiltonian linear in the momentum as

$$H(\mathbf{p}) = \begin{pmatrix} 0 & vp_+ \\ vp_- & 0 \end{pmatrix}, \tag{1}$$

where v is a constant of the velocity units. The same Hamiltonian was written using the tight-binding model.

The eigenvalues of this matrix give two bands

$$\varepsilon_{1,2} = \mp v\sqrt{p_x^2 + p_y^2} = \mp vp,$$

where the sign $\mp$ corresponds to holes and electrons. The gapless linear spectrum arises as a consequence of the symmetry, and the chemical potential at zero temperatures coincides with the band crossing due to the carbon valence. The cyclotron mass has the form

$$m(\varepsilon) = \frac{1}{2\pi}\frac{dS(\varepsilon)}{d\varepsilon} = \frac{\varepsilon}{v^2},$$

and the carrier concentration at zero temperature $n(\mu) = \mu^2/\pi\hbar^2 v^2$ is expressed in terms of the chemical potential μ.

Tuning the gate voltage, the linearity of the spectrum has been examined in the Schubnikov–de Haas studies[27] with the help of the connection between the effective mass and the carrier concentration at the Fermi level $m(\mu)v = \mp\hbar\sqrt{\pi n(\mu)}$. The "constant" parameter v was found to be no longer constant, but at low carrier concentrations $n \sim 10^9$ cm^{-2}, it exceeds its usual value $v = 1.05 \pm 0.1 \times 10^8$ cm/s (at concentrations $n > 10^{11}$ cm^{-2}) by the factor of 3.

This is a result of electron-electron interactions which become stronger at low carrier concentrations. The logarithmic renormalization of the velocity was found by Abrikosov and Beneslavsky in Ref.[28] for the 3d case and in Refs.[29,30] for 2d graphene. Notice, that no phase transition was revealed even at lowest carrier concentration. We can conclude that the Coulomb interactions do not create any gap in the spectrum.

B. Electron dispersion in bilayer graphene and graphite

Bilayer graphene has attracted much interest partly due to the opening of a tunable gap in its electronic spectrum by an external electrostatic field. Such a phenomenon was predicted in Refs.[31,32] and was observed in optical studies controlled by applying a gate voltage[33–40].

The graphene bilayer lattice is shown in Fig. 2. Atoms in one layer, i. e., **a** and **b** in the unit cell, are connected by solid lines, and in the other layer, e. g., **a₁** and **b₁**, by the dashed lines. The atom **a** (**a₁**) differs from **b** (**b₁**) because it has a neighbor in the adjacent layer, whereas the atom **b** (**b₁**) does not.
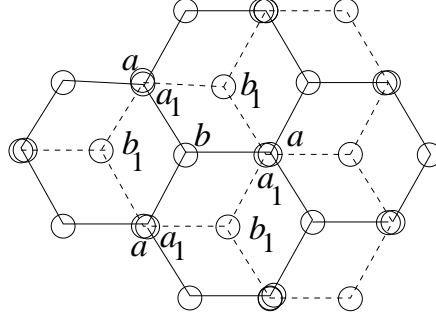

Figure 2: Bilayer lattice

The effective Hamiltonian of the SWMC theory can be written[22,23] near the KH line in graphite as

$$
H(\mathbf{p}) = \begin{pmatrix}
\tilde{\gamma}_5 & vp_+ & \tilde{\gamma}_1 & \tilde{\gamma}_4 vp_-/\gamma_0 \\
vp_- & \tilde{\gamma}_2 & \tilde{\gamma}_4 vp_-/\gamma_0 & \tilde{\gamma}_3 vp_+/\gamma_0 \\
\tilde{\gamma}_1 & \tilde{\gamma}_4 vp_+/\gamma_0 & \tilde{\gamma}_5 & vp_- \\
\tilde{\gamma}_4 vp_+/\gamma_0 & \tilde{\gamma}_3 vp_-/\gamma_0 & vp_+ & \tilde{\gamma}_2
\end{pmatrix},
\tag{2}
$$

where $p_\pm = \mp ip_x - p_y$ are the momentum components and $\tilde{\gamma}_j$ are the functions of the p_z momentum in the major axis direction,

$$
\tilde{\gamma}_2 = 2\gamma_2 \cos\left(2p_z d_0\right), \tilde{\gamma}_5 = 2\gamma_5 \cos\left(2p_z d_0\right) + \Delta,
$$

$$
\tilde{\gamma}_i = 2\gamma_i \cos\left(p_z d_0\right) \quad \text{for} \quad i = 1, 3, 4,
$$

with the distance $d_0 = 3.35$ Å between layers in graphite. The nearest-neighbor hopping integral $\gamma_0 \approx 3$ eV corresponds with the velocity parameter $v = 1.5a_0\gamma_0 = 10^6$ m/s and the in-layer inter atomic distance $a_0 = 1.415$ Å. The Hamiltonian (2) is represented in a somewhat different form than that in Ref.[1]. The relations between the hopping integrals in these forms are given in Table I. The recent estimate[35,36] of the parameters agrees with those given in the Table.

The electron spectrum of graphite is shown in Fig. 3. There are four levels labeled by the number $s = 1, 2, 3, 4$ from below at any momentum. As a consequence of axial symmetry, twofold degeneration $\varepsilon_2 = \varepsilon_3$ exists at $p_x = p_y = 0$, i. e., on the KH line.

Table I: The parameters of the Hamiltonian, Eq. (2), their values in the SWMC model, and obtained in the experimental works, all in meV.

Eq. (2)	γ_0	γ_1	γ_2	γ_3	γ_4	γ_5	Δ	ε_F
	3050	360	-10.2	270	-150	-1.5	16	-4.1
S[a]	γ_0	γ_1	$2\gamma_2$	γ_3	$-\gamma_4$	$2\gamma_5$	$\Delta + 2(\gamma_2 - \gamma_5)$	$2\gamma_2 + \varepsilon_F$
M[b]	3160	390	-20	276	44	38	8	-24
D[c]	3120	380	-21	315	120	-3	-2	$-$
DFT[d]	2598±15	340±20	-	320±20	177±25	-	24±10	-

[a]SWMC,Ref.[1], [b]Mendez et al, Ref.[5], [c]Doezema et al, Ref.[4]. [d]Charlier et al, Ref.[42].
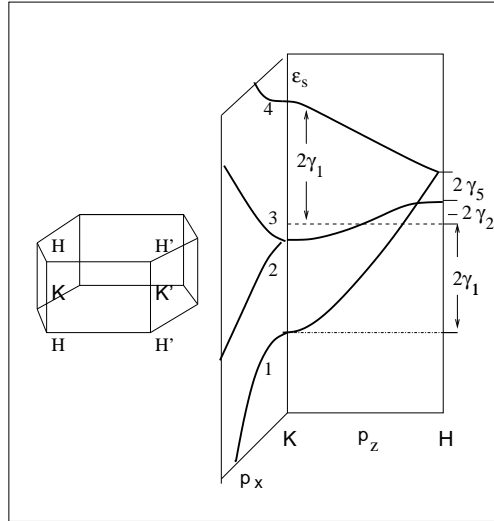

Figure 3: Band structure of graphite

In bilayer graphene, every layer has only one neighboring layer. Therefore, we have to set $\gamma_2 = \gamma_5 = 0$ and to substitute $\tilde{\gamma}_i = \gamma_i$ for $i = 1, 3, 4$ in Hamiltonian (2). The parameter U can be included also in the bilayer Hamiltonian as a result of the gate voltage. Then, the gap appears between the ε_2 and ε_3, and these bands acquire the form of "mexican hat". An important point is that two points, K and K', are in the Brillouin zone transforming each in other under reflection. Such a reflection changes the U sign giving two different dispersion laws at the K and K' points.

III. OPTICAL CONDUCTIVITY

We use the general expression for the conductivity as a function of the electric field frequency ω and wave vector k in the form[43,44]

$$\sigma_{ij}(\omega, k) =$$
$$2ie^2 \sum_{\mathbf{p}, m>n} \left\{ \frac{v_{mm}^i v_{mm}^j \{f_0[\varepsilon_m(\mathbf{p}_-)] - f_0[\varepsilon_m(\mathbf{p}_+)]\}}{[\varepsilon_m(\mathbf{p}_+) - \varepsilon_m(\mathbf{p}_-)][\omega - \varepsilon_m(\mathbf{p}_+) + \varepsilon_m(\mathbf{p}_-)]} \right. \tag{3}$$
$$\left. + 2\omega \frac{v_{mn}^i v_{nm}^j \{f_0[\varepsilon_m(\mathbf{p}_-)] - f_0[\varepsilon_n(\mathbf{p}_+)]\}}{[\varepsilon_n(\mathbf{p}_+) - \varepsilon_m(\mathbf{p}_-)]\{(\omega + i\delta)^2 - [\varepsilon_n(\mathbf{p}_+) - \varepsilon_m(\mathbf{p}_-)]^2\}} \right\} ,$$

valid in the collisionless limit $(\omega, kv) \gg \tau^{-1}$, where τ^{-1} is the electron relaxation frequency, $\mathbf{p}_\pm = \mathbf{p} \pm \mathbf{k}/2$, and v_{mn}^i is the matrix element of the velocity operator

$$\mathbf{v} = \partial H(\mathbf{p})/\partial \mathbf{p} \tag{4}$$

determined by Hamiltonians (1) or (2). Hitherto, we did not use any peculiarities of the graphene spectrum The expression acquired only the factor 4 due to summation over spin and over six points of the K type (two per the Brillouin zone).

The first term in Eq. (3) corresponds to the intraband electron-photon scattering processes. In the limit of the high carriers concentration $(T, E_F) \gg kv$, it coincides with the usual Drude–Boltzmann conductivity, if the substitution $\omega \to \omega + i\tau^{-1}$ is made. The second term owes its origin to the interband $n \to m$ transitions with the infinitesimal δ determining the bypass around the pole while integrating over the momentum $\mathbf{p}$. The real part of this contribution is reduced to the well-known expression for the absorbed energy due to direct interband transitions.

A. Optical conductivity of graphene

For optical frequencies $\omega \gg kv$, we can integrate in Eq. (3) over the angle and write the conductivity as

$$\sigma(\omega) = \frac{e^2 \omega}{i\pi\hbar} \left[\int_{-\infty}^{+\infty} d\varepsilon \frac{|\varepsilon|}{\omega^2} \frac{df(\varepsilon)}{d\varepsilon} - \int_0^{+\infty} d\varepsilon \frac{f(-\varepsilon) - f(\varepsilon)}{(\omega + i\delta)^2 - 4\varepsilon^2} \right] \tag{5}$$

using the variable $\varepsilon = vp$.

The intraband term can be integrated once more,

$$\sigma^{intra}(\omega) = \frac{2ie^2 T}{\pi\hbar(\omega + i\tau^{-1})} \ln\left(2\cosh\frac{\mu}{2T}\right),$$ (6)

where we write $\omega + i\tau^{-1}$ instead of ω to take the small relaxation frequency into account. This Drude–Boltzmann conductivity at low temperatures $T \ll \mu$ takes the form

$$\sigma^{intra}(\omega) = \frac{ie^2|\mu|}{\pi\hbar(\omega + i\tau^{-1})}.$$ (7)

In the opposite limit of high temperatures, the intraband conductivity Eq. (6) becomes

$$\sigma^{intra}(\omega) = \frac{2ie^2 T \ln 2}{\pi\hbar(\omega + i\tau^{-1})}.$$ (8)

The temperature dependence of the relaxation rate in graphene is discussed theoretically in Ref.[51].

The interband contribution in Eq. (5) integrated at zero temperatures gives

$$\sigma^{inter}(\omega) = \frac{e^2}{4\hbar}\left[\theta(\omega - 2\mu) - \frac{i}{2\pi}\ln\frac{(\omega + 2\mu)^2}{(\omega - 2\mu)^2}\right],$$ (9)

where the $\theta-$function expresses the threshold behavior of interband electron transitions at $\omega = 2\mu$. The temperature smooths out all the singularities

$$\theta(\omega - 2\mu) \to \frac{1}{2} + \frac{1}{\pi}\arctan\frac{\omega - 2\mu}{2T}$$ (10)
$$(\omega - 2\mu)^2 \to (\omega - 2\mu)^2 + (2T)^2.$$

The main issue should be emphasized. In high frequency region $\omega \gg (T, \mu)$, the iterband transitions make the main contribution into conductivity

$$\sigma(\omega) = \frac{e^2}{4\hbar},$$

having the universal character independent of any material parameters. This frequency region is limited above by the band width of around 3 eV. Making use the universal conductivity, one can calculate the light transmission through graphene[46] in the approximation linear in conductivity

$$T = 1 - \frac{4\pi}{c}Re\,\sigma(\omega)\cos\theta = 1 - \pi\frac{e^2}{\hbar c}\cos\theta,$$ (11)

where θ is the incidence angle. The intensity of reflected light is quadratic in the fine structure constant $\alpha = e^2/\hbar c$. In excellent agreement with the theory, for the wide optical

range, several experimental groups[47–49] observe the light transmission through graphene as well as bilayer graphene where the difference from unity is twice as larger. It is exceptionally intriguing that the light transmission involves the fine structure constant of quantum electrodynamics having really no relations to the graphene physics.

For graphite, the value of $\sigma_d = e^2/4\hbar d_0$ plays the role of the universal dynamical conductivity, where d_0 is the distance between layers. As shown experimentally[50] and theoretically[51], the dynamical conductivity of graphite is close to this universal value in the frequency range 0.1–1 eV having the kink singularity at the interband transition frequency $\omega = 2\gamma_1$.

IV. GRAPHENE IN MAGNETIC FIELDS

In the presence of the magnetic field B, the momentum projections p_+ and p_- become the operators with the commutation rule $\{\hat{p}_+, \hat{p}_-\} = -2e\hbar B/c$. We use the relations

$$v\hat{p}_+ = \omega_B\, a, \quad v\hat{p}_- = \omega_B\, a^+$$

involving the creation a^+ and annihilation a operators with $\omega_B = v\sqrt{2|e|\hbar B/c}$. We will write only one of two x, y space coordinates including the corresponding degeneracy proportional to the magnetic field in the final results.

For graphene, we search the eigenfunction of Hamiltonian (1) in the form

$$\psi_{sn}^\alpha(x) = \begin{cases} C_{sn}^1 \varphi_{n-1}(x) \\ C_{sn}^2 \varphi_n(x) \end{cases}, \tag{12}$$

where $\varphi_n(x)$ are orthonormal Hermitian functions with the Landau number $n \geq 0$. Canceling the Hermitian functions from the equations, we obtain a system of linear equations for the eigenvector $\mathbf{C}_{sn}$

$$\begin{pmatrix} -\varepsilon & \omega_B\sqrt{n} \\ \omega_B\sqrt{n} & -\varepsilon \end{pmatrix} \times \begin{cases} C_{sn}^1 \\ C_{sn}^2 \end{cases} = 0 \tag{13}$$

giving the eigenvalues

$$\varepsilon_{sn} = \mp\omega_B\sqrt{n}$$

with $s = 1, 2$ and $n = 0, 1, 2...$ For $n = 0$, there is only one level $\varepsilon_{10} = 0$ with $C_0^1 = 0, C_0^2 = 1$

as follows from Eq. (12). The wave function columns write

$$
\begin{matrix} C^1_{sn} \\ C^2_{sn} \end{matrix} = \frac{1}{\sqrt{2}} \left\{ \begin{matrix} 1 \\ -1 \end{matrix} \right. \quad \text{and} \quad \begin{matrix} 1 \\ 1 \end{matrix} \tag{14}
$$

for $s = 1$ and $s = 2$ and $n = 1, 2....$

V. GRAPHENE LAYERS WITH TRIGONAL WARPING IN MAGNETIC FIELDS

We search the eigenfunction of Hamiltonian (2) as a column

$$
\psi^\alpha_{sn}(x) = \left\{ \begin{matrix} C^1_{sn}\varphi_{n-1}(x) \\ C^2_{sn}\varphi_n(x) \\ C^3_{sn}\varphi_{n-1}(x) \\ C^4_{sn}\varphi_{n-2}(x) \end{matrix} \right. . \tag{15}
$$

One sees the every row in Hamiltonian (2) becomes proportional to the definite Hermitian function if the terms with γ_3 are omitted. We will show that the terms proportional to γ_3/γ_0 can be considered within the perturbation theory or the semiclassical approximation.

Canceling the Hermitian functions from the equations, we obtain a system of the linear equations for the eigenvector $\mathbf{C}_{sn}$

$$
\begin{pmatrix} \tilde{\gamma}_5 - \varepsilon & \omega_B\sqrt{n} & \tilde{\gamma}_1 & \omega_4\sqrt{n-1} \\ \omega_B\sqrt{n} & \tilde{\gamma}_2 - \varepsilon & \omega_4\sqrt{n} & 0 \\ \tilde{\gamma}_1 & \omega_4\sqrt{n} & \tilde{\gamma}_5 - \varepsilon & \omega_B\sqrt{n-1} \\ \omega_4\sqrt{n-1} & 0 & \omega_B\sqrt{n-1} & \tilde{\gamma}_2 - \varepsilon \end{pmatrix} \times \left\{ \begin{matrix} C^1_{sn} \\ C^2_{sn} \\ C^3_{sn} \\ C^4_{sn} \end{matrix} \right. = 0 , \tag{16}
$$

where the band number $s = 1, 2, 3, 4$ numerates the solutions at given n from the bottom, $\omega_B = v\sqrt{2|e|\hbar B/c}$ and $\omega_4 = \tilde{\gamma}_4\omega_B/\gamma_0$.

The eigenvalues of the matrix in Eq. (16) are easily found, they are shown in Fig. 4 as a function of the momentum p_z. For each Landau number $n \geq 2$ and momentum p_z, there are four eigenvalues $\varepsilon_s(n)$ and four corresponding eigenvectors, Eq. (15), marked by the band subscript s. We use the notation $|sn\rangle$ for levels. In addition, there are four levels. One of them is
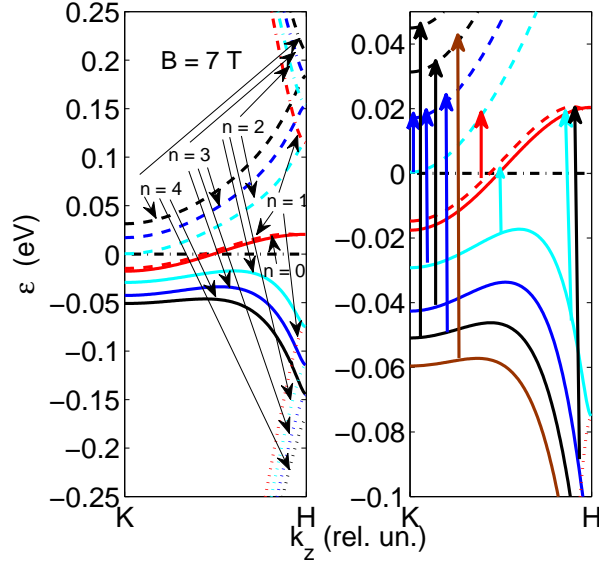
$$
\varepsilon_1(n = 0) = \tilde{\gamma}_2 \tag{17}
$$

Figure 4: (Color online) Landau levels in graphite ε_{sn} for n from 0 to 4 in four bands $s =$1,2,3, and 4 (in dotted, solid, dashed, and dash-dotted lines, correspondingly) as functions of wave vector k_z along the KH line in the Brillouin zone ($K = 0$, $H = \pi/2d_0$) in the magnetic field $B = 7$ T with the SWMC model parameters given in Table 1.The main electron transitions shown in the right panel below 100 meV occur between the levels with the selection rule $\Delta n = 1$, see text.

for $n = 0$ with the eigenvector $\mathbf{C}_0 = (0, 1, 0, 0)$ as is evident from Eq. (15). It intersects the Fermi level and belongs to the electron (hole) band near the K (H) point. The other three levels indicated with $n = 1$ and $s = 1, 2, 3$ are determined by the first three equations of the system (16) with $C_{s1}^4 = 0$.

The $|21\rangle$ level is close to the $|10\rangle$ level. In the region of p_z, $\gamma_1/\cos 2p_z d_0 \gg \gamma_2$, where the electrons are located, this level has the energy

$$\varepsilon_2(n = 1) = \tilde{\gamma}_2 - 2\frac{\omega_B^2 \tilde{\gamma}_4}{\tilde{\gamma}_1 \gamma_0}.$$

In the same region, the two closest bands ($s = 2, 3$) with $n \geq 2$ are written as

$$\varepsilon_{2,3}(n) = \tilde{\gamma}_2 - \frac{\omega_B^2 \tilde{\gamma}_4}{\tilde{\gamma}_1 \gamma_0}(2n - 1) \mp \frac{\omega_B^2}{\tilde{\gamma}_1}\sqrt{n(n - 1)} \tag{18}$$

within accuracy of $(\tilde{\gamma}_4/\gamma_0)^2$.

A. Perturbation theory for matrix Hamiltonian

Due to a double degeneracy existing on the KH line, the effect of the trigonal warping becomes essential. A simplest way[16] to evaluate the corrections resulting from the warping γ_3 consists in the consideration of the Green's function having the poles at the electron levels.

The Green's function of the unperturbed Hamiltonian writes using the functions in Eq. (15) as

$$G_0^{\alpha\beta}(\varepsilon, x, x') = \sum_{sn} \frac{\psi_{sn}^{\alpha}(x)\psi_{sn}^{*\beta}(x')}{\varepsilon - \varepsilon_{sn}}. \tag{19}$$

The corrections to the levels can be found in the iterations

$$\mathbf{G}_{m+1}(x, x') = \int d^2x'' \mathbf{G}_0(x, x'') \mathbf{V}(x'') \mathbf{G}_m(x'', x'), \tag{20}$$

where $\mathbf{V}(\mathbf{x})$ has only two matrix elements $V^{42} = \omega_B \tilde{\gamma}_3 a^+/\gamma_0$ and $V^{24} = V^{42*}$ in the Hamiltonian (2).

In the second iteration, we get the corrections

$$\int d^2x_1 d^2x_2 G_0^{\alpha 4}(x, x_1) V^{42}(x_1) G_0^{22}(x_1, x_2) V^{24}(x_2) G_0^{4\beta}(x_2, x')$$

and the similar term with the superscript substitution $2 \leftrightarrow 4$. The matrix elements of the perturbation V are easily calculated with respect to the Hermitian functions in Eqs. (19) and (15), and we obtain

$$\left(\frac{\omega_B \tilde{\gamma}_3}{\gamma_0}\right)^2 \sum_{s'sn} \frac{(n-2)|C_{sn}^4 C_{s',n-3}^2|^2 \psi_{sn}^{\alpha}(x)\psi_{sn}^{*\beta}(x')}{(\varepsilon - \varepsilon_{sn})(\varepsilon - \varepsilon_{s',n-3})(\varepsilon - \varepsilon_{sn})}. \tag{21}$$

for the diagram shown in the upper part of Fig. 5. This correction plays an important role near the poles of the Green's function. For this reason, for ε close to ε_{sn}, the ε value in the second factor of the denominator can be replaced by ε_{sn}. Thus, the total Green's function (with the correction) has the structure

$$\frac{1}{\varepsilon - \varepsilon_{sn}} + \frac{\delta}{(\varepsilon - \varepsilon_{sn})^2},$$

which can be rewritten to the second-order terms in δ as

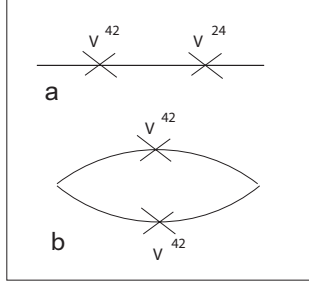$$\frac{1}{\varepsilon - \varepsilon_{sn} - \delta}.$$

Figure 5: Diagrams for the second iteration of the perturbation theory; corrections to the Green's function (a), corrections to the vertex in conductivity (b).

Therefore, we can represent the correction as a shift $\delta\varepsilon_{sn}$ of the poles $(\varepsilon - \varepsilon_{sn} - \delta\varepsilon_{sn})^{-1}$ with

$$
\delta\varepsilon_s(n) = \left(\frac{\omega_B\tilde{\gamma}_3}{\gamma_0}\right)^2 \sum_{s'} \left\{ \frac{(n-2)|C_{sn}^4 C_{s',n-3}^2|^2}{\varepsilon_s(n) - \varepsilon_{s'}(n-3)} + \frac{(n+1)|C_{sn}^2 C_{s',n+3}^4|^2}{\varepsilon_s(n) - \varepsilon_{s'}(n+3)} \right\},
$$

(22)

where the first term should be omitted for $n - 3 < 0$. In fact, our illustration is nothing but a calculation of the electron self-energy and the naive expansion of the denominator can indeed be replaced by summarizing of the corresponding diagrams.

The corrected $|10\rangle$ level writes

$$
\varepsilon_1(n=0) = \tilde{\gamma}_2 + \left(\frac{\omega_B\tilde{\gamma}_3}{\gamma_0}\right)^2 \sum_{s'} \frac{|C_{s'3}^4|^2}{\tilde{\gamma}_2 - \varepsilon_{s'}(3)}.
$$

(23)

The $|21\rangle-$level is very close to the level with $n = 0$, Eq. (23).

Comparing the corrections, Eq. (22), with the main contribution Eq. (18), we find, first, that the perturbation theory is valid when an expansion parameter $(\tilde{\gamma}_3\tilde{\gamma}_1/\gamma_0\omega_B)^2$ becomes small, i.e., for strong magnetic fields $B > 1\,T$. Second, the effect of γ_4 is linear, whereas of γ_3 is quadratic in these constants. Therefore, the γ_4 constant is more essential for the electron levels in magnetic fields.

Comparison shows that Eqs. (22) and (23) for levels give the same results as the numerical method of truncating the infinite-rink matrix in Ref.[21].

Note that the derived expressions are applicable as well to bilayer graphene while one includes the field U and substitutes $\gamma_2 = \gamma_5 = 0$ and $\tilde{\gamma}_i = \gamma_i$ for $i = 1, 3, 4$. In the simplest approach, when only main parameters γ_1 and U are holded, the magnetic levels ε_{sn} are

determined by the equation

$$[(U - \varepsilon_{sn})^2 - \omega_B^2 n][(U + \varepsilon_{sn})^2 - \omega_B^2(n+1)] + \gamma_1^2(U^2 - \varepsilon_{sn}^2) = 0\,.$$

B. Berry phase, semiclassical quantization and Landau levels

Alternatively, the semiclassical quantization can be applied for relatively weak magnetic fields when the cyclotron frequency is small compared to the Fermi energy. Then, we can use the Bohr–Zommerfeld condition as

$$\frac{c}{e\hbar B}S(\varepsilon) = 2\pi\left[n_c + \frac{\mathcal{T}}{4} + \delta(\varepsilon)\right]\,. \tag{24}$$

Here $S(\varepsilon)$ is the cross-section area of the electron orbit in the $p_x.p_y$ space for the energy ε and the constant momentum projection p_z on the magnetic field, n_c is an integer supposed to be large. The integer $\mathcal{T}$ is the number of the smooth turning points on the electron orbit. There are two smooth turning points for the Landau levels and only one for skipping electrons reflected by the hard edge.

We use the semiclassical approach for the magnetic field normal to the layered system when the in-layer momentum components p_x and p_y are only quantized and the size of the Fermi surface is small compared with the Brillouin zone size. Notice, that the $\delta(\varepsilon)$-phase depends on the energy. If the spin is neglected, $\delta = 0$ and $\mathcal{T} = 2$ for the Landau levels, and $\delta = 1/2$ and $\mathcal{T} = 2$ for monolayer graphene. In these two cases, the semiclassical result coincides with the rigorous quantization and it is closely connected with the topological Berry phase[52]. This δ-phase was evaluated for bismuth in Ref.[25], preceding Berry's work by almost two decades, and it was considered again for bismuth in Ref.[53]. For graphite, the semiclassical quantization was applied in Ref.[26]. However, in the general case, the evaluation of the $\delta-$phase is still attracted a widespread interest[54–60].

The problem under consideration is described by the Hamiltonian in Eqs. (1) or (2) rewritten in the form

$$(\mathbf{V} \cdot \tilde{\mathbf{p}} + \Gamma - \varepsilon)\Psi = 0\,, \tag{25}$$

where $\tilde{\mathbf{p}}$ and $\mathbf{V}$ are the two-dimensional vector and matrix, correspondingly, with the in-layer components x and y. The column Ψ is labeled by the band subscript which we omit together with the matrix subscripts on Γ and $\mathbf{V}$, summation over them is implied in Eq.

(25). Matrices Γ and $\mathbf{V}$ are the first two terms (of zero and first orders) in a series expansion of the Hamiltonian in the power of quasi-momentum p_x and p_y.

In the magnetic field, the momentum operator $\tilde{\mathbf{p}}$ depends on the vector-potential $\mathbf{A}$ by means of the Peierls substitution,

$$\tilde{\mathbf{p}} = -i\hbar\nabla - e\mathbf{A}/c,$$

providing the gauge invariance of the theory. The magnetic field can also enter explicitly describing the magnetic interaction with a spin of particles. However, for the graphene family, the magnetic interaction is weak and omitted here.

It is convenient to choose the vector-potential in the Landau gauge $A_x = -By, A_y = A_z = 0$ in such a way that the Hamiltonian does not depend on the x coordinate. We search the function Ψ in the form

$$\Psi = \Phi\exp\left(is/\hbar\right),$$

where the function s is assumed to be common for all component of the column Ψ.

The function Φ is expanding in series of $\hbar/i$:

$$\Phi = \sum_{m=0}^{\infty} \left(\frac{\hbar}{i}\right)^m \varphi_m \,.$$

Collecting the terms with the same powers of $\hbar$ in Eq. (25), we have

$$(\mathbf{V}\cdot\mathbf{p} + \Gamma - \varepsilon)\varphi_m = -\mathbf{V}\nabla\varphi_{m-1} \,. \tag{26}$$

For $m = 0$, we get a homogeneous system of algebraic equations for the wave function column φ_0,

$$(\mathbf{V}\cdot\mathbf{p} + \Gamma - \varepsilon)\varphi_0 = 0\,, \tag{27}$$

which has a solution under the condition

$$\mathrm{Det}(\mathbf{V}\cdot\mathbf{p} + \Gamma - \varepsilon) = 0\,. \tag{28}$$

This equation determines the classical electron orbit, $\varepsilon(p_x, p_y) = \varepsilon$, at the given electron energy ε in presence of the magnetic field. On the other hand, the equation coincides with the dispersion equation since it does not contain the magnetic field. In 3d case, as in graphite, the dispersion depends also on the momentum projection p_z on the magnetic field. Thus, our scheme does not requires the expansion in a power of p_z.

15

The equations (26) with $m = 0, 1$ give the wave function in the semiclassical approximation[25]. The quantization condition can be written as usual from the requirement that the wave function has to be single-valued. Making the bypass in the complex plane around the turning points to obtain the decreasing solutions in the classically unaccessible region, we obtain, first, $\mathcal{T} = 2$ and, second, δ-phase as a contour integral along the classical orbit

$$\delta(\varepsilon) = \frac{1}{2\pi} \text{Im} \oint \frac{dp_x}{\varphi_0^* \varphi_0 v_y} \varphi_0^* V_y \frac{d\varphi_0}{dp_x},$$
(29)

where $v_y = \partial \varepsilon(p_x, p_y) / \partial p_y$. Using the Hamiltonian hermiticity, after the simple algebra (see Ref.[25]), Eq. (29) can be rewrite in the gauge-invariant form

$$\delta(\varepsilon) = \frac{1}{4\pi} \text{Im} \oint \frac{dp}{\varphi_0^* \varphi_0 v} \varphi_0^* \left[\mathbf{V} \times \frac{d}{d\mathbf{p}} \right]_z \varphi_0.$$
(30)

where $v = \sqrt{v_x^2 + v_y^2}$ and the integrand is called the Berry connection (or curvature). Everywhere, the summation over the band subscript is implied.

Now let us calculate the δ-phase for bilayer graphene. In the simplest case, omitting γ_3 and γ_4, the effective Hamiltonian can be written as

$$H(\mathbf{p}) = \begin{pmatrix} U & q_+ & \gamma_1 & 0 \\ q_- & U & 0 & 0 \\ \gamma_1 & 0 & -U & q_- \\ 0 & 0 & q_+ & -U \end{pmatrix},$$
(31)

where the parameter U describes the tunable gap as a result of the gate voltage and γ_1 is the interlayer nearest-neighbor hopping integral energy.The constant velocity parameter v is incorporated in the notation $q_\pm = v p_\pm$. The band structure is shown in Fig. 6. The minimal value of the upper energy ε_4 is $\sqrt{U^2 + \gamma_1^2}$, the ε_3 band takes the maximal value $|U|$ at $q = 0$. Here, the orbit is the circle defined by Eq. (28), written in the form

$$[(U + \varepsilon)^2 - q^2][(U - \varepsilon)^2 - q^2] - \gamma_1^2(\varepsilon^2 - U^2) = 0.$$
(32)

The eigenfunction φ_0 of the Hamiltonian (31) can be taken as

$$\varphi_0 = \begin{pmatrix} (U - \varepsilon)[(\varepsilon + U)^2 - q^2] \\ q_-[q^2 - (\varepsilon + U)^2] \\ \gamma_1(U^2 - \varepsilon^2) \\ \gamma_1 q_+(U - \varepsilon) \end{pmatrix},$$
(33)

16

with the norm squared

$$\varphi_0^* \varphi_0 = [(\varepsilon + U)^2 - q^2]^2 [(\varepsilon - U)^2 + q^2]$$
$$+ \gamma_1^2 (\varepsilon - U)^2 [(\varepsilon + U)^2 + q^2] . \tag{34}$$

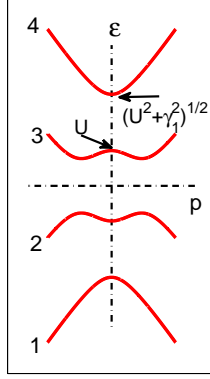The derivatives for Eq. (29) are calculated along the trajectory where the energy ε and, consequently, the trajectory radius q are constant.

Figure 6: Band structure of bilayer graphene

If the conditions $|U| < |\varepsilon| < \sqrt{U^2 + \gamma_1^2}$ are fulfilled, Eq. (32) has only one solution for the radius squared

$$q^2 = U^2 + \varepsilon^2 + \sqrt{4U^2\varepsilon^2 + (\varepsilon^2 - U^2)\gamma_1^2} .$$

The matrix $V_y = \partial H / \partial p_y$ in Eq. (29) has four nonzero elements, $V_y^{12} = V_y^{21} = V_y^{34} = V_y^{43} = -1$.

Using Eqs. (32) and (33), we find

$$\text{Im } \varphi_0^* V_y \frac{d\varphi_0}{dp_x} = 4U\varepsilon(U - \varepsilon)[(\varepsilon + U)^2 - q^2] . \tag{35}$$

This expression is constant on the trajectory as well as $\varphi_0^* \varphi_0$, Eq. (34). Therefore, in order to find δ, Eq. (29), we have to integrate along the trajectory

$$\oint \frac{dp_x}{v_y} .$$

This integral equals $-dS(\varepsilon)/d\varepsilon$, where $S(\varepsilon) = \pi q^2$ is the cross-section area, Eq. (24), with

$$\frac{dS(\varepsilon)}{d\varepsilon} = \pi\varepsilon \frac{2(q^2 + U^2 - \varepsilon^2) + \gamma_1^2}{q^2 - U^2 - \varepsilon^2} . \tag{36}$$

17

Now we have to substitute Eqs. (34) – (36) into Eq. (29). Thus, we find the Berry phase

$$\delta(\varepsilon) = \frac{-\varepsilon U}{q^2 - \varepsilon^2 - U^2} = \frac{-\varepsilon U}{\sqrt{4U^2\varepsilon^2 + (\varepsilon^2 - U^2)\gamma_1^2}} \tag{37}$$

shown in Fig. 7, where δ-phase of bilayer graphene with trigonal warping is also shown; the detailed calculations will be published elsewhere. For the ungaped bilayer, $U = 0$, the Berry phase $\delta(\varepsilon) = 0$. The Berry phase depends on the energy and $\delta = \mp 1/2$ at $\varepsilon = \pm U$. At the larger energy, $\varepsilon \gg U$, the Berry phase $\delta \to \mp U/\gamma_1$.

Substituting Eq. (37) in the semiclassical quantization condition, Eq. (24), and solving the equation obtained for ε, we get the energy levels as functions of the magnetic field. We have to notice that the Landau numbers n listed in Fig. 8 do not coincide with the numbers n_c in the semiclassical condition (24). The rigorous quantization shows that there are only one Landau level with $n = 0$ and three Landau levels with $n = 1$[16]. These levels are not correctly described within the semiclassical approach. However, for $n \geq 2$, there are levels in all four bands s (two nearest bands with $s = 2, 3$ are shown in Fig. 8). They correspond with the semiclassical number $n_c = n - 1$, and the semiclassical levels for the larger n are in excellent agreement with the levels obtained in the perturbation approximation.
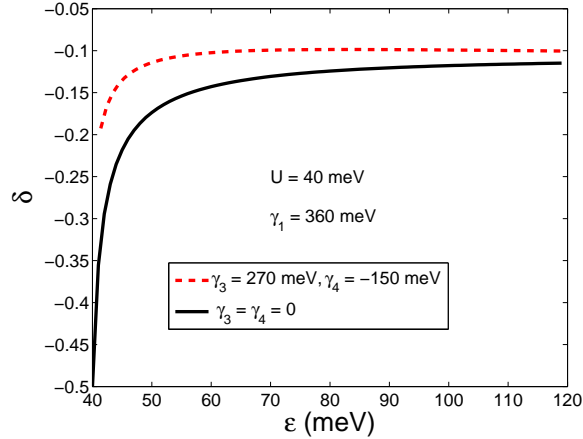

Figure 7: (Color online) Semiclassical phase vs energy in the conduction band of bilayer graphene without trigonal warping (solid line) and with warping (dashed line).

VI. MAGNETO-OPTICS EFFECTS IN GRAPHENE LAYERS

An important peculiarity of conductivities in presens of magnetic fields is an appearance of the Hall component $\sigma_{xy}(\omega)$. The Hall conductivity violates the rotation symmetry of graphene around the major axis. This implies the rotation of the linear polarized electromagnetic wave, i. e., the Faraday and Kerr effects for transmitted and reflected waves, correspondingly. First of all, the electron transitions are possible between the levels with the neighboring Landau numbers n and various bands s, and therefore the resonance denominators $\Delta_{ss'n} = \varepsilon_{sn} - \varepsilon_{s',n+1}$ arise in the conductivity tensor.

Calculations[16] give the conductivities for graphite in the collisionless limit when the electron collision frequency Γ is much less than the level splitting

$$
\left.\begin{array}{c} \sigma_{xx}(\omega) \\ i\sigma_{xy}(\omega) \end{array}\right\} = i\sigma_d \frac{4\omega_B^2}{\pi^2} \sum_{n,s,s'} \int\limits_0^{\pi/2} dz \frac{\Delta f_{ss'n}}{\Delta ss'n} |d_{ss'n}|^2 \tag{38}
$$
$$
\times \left[(\omega + i\Gamma + \Delta_{ss'n})^{-1} \pm (\omega + i\Gamma - \Delta_{ss'n})^{-1} \right],
$$

where the integration is taken over the reduced Brillouin zone, $0 < z < \pi/2$. Such integration is absent for graphene and bilayer. Here $\Delta f_{ss'n} = f(\varepsilon_{s'n+1}) - f(\varepsilon_{sn})$ is the difference of the
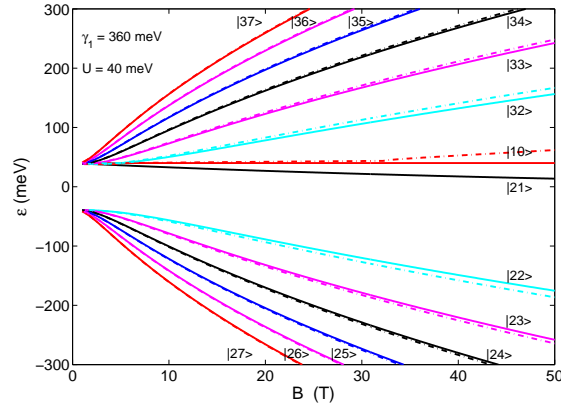

Figure 8: (Color online) Energy levels ε_{sn} for the K valley in magnetic fields for bilayer graphene within the perturbation approximation (solid lines) and in the semiclassical approach (dashed-dotted lines); in the notation $|sn\rangle$, n is the Landau number and $s = 1, 2, 3, 4$ is the band number, only two nearest bands ($s = 2, 3$) are shown at given n from 0 to 7. There is only one level, $|10\rangle$, with $n = 0$ and three levels ($s = 1, 2, 3$) with $n = 1$. The levels for the K' valley can be obtained by mirror reflection with respect to the $\varepsilon = 0$ axis.

Fermi functions and

$$d_{ss'n} = C_{sn}^2 C_{s'n+1}^1 + C_{sn}^3 C_{s'n+1}^4$$
$$+ (\tilde{\gamma}_4/\gamma_0)(C_{sn}^1 C_{s'n+1}^4 + C_{sn}^2 C_{s'n+1}^3)$$

is the dipole matrix element expressed in terms of wave functions (15). These transitions are most intensive. They obey the the selection rule

$$\Delta n = 1\,,$$

and will be referenced as the strong lines. The conductivity units here

$$\sigma_d = \frac{e^2}{4\hbar d_0}$$

have a simple meaning, being the graphene universal conductivity $e^2/4\hbar$ multiplied by the number $1/d_0$ of layers within the distance unit in the major axis direction.

Besides, we have to take the renormalization of the dipole moments due to trigonal warping into account. This additional electron-photon vertex results in weak lines with the selection rule

$$\Delta n = 2.$$

We get this contribution by substituting

$$d_{ss'n} = (\tilde{\gamma}_3/\gamma_0) C_{sn}^2 C_{s'n+2}^4$$

instead of the matrix element in Eq. (38) and replacing the subscript $n + 1 \to n + 2$. We have to notice, that the γ_4 corrections give the linear (in small parameter γ_4/γ_0) contribution to the conductivities at the main electron transitions with $\Delta n = 1$. The γ_3 corrections are quadratic, however, they result in an appearance of new resonant transitions with $\Delta n = 2$.

There are also small so-called vertex corrections to the self-energy shown at the bottom of Fig. 5. They result from the quartet of the coupled Landau levels, which interfere while the selection rules $\Delta n = 1$ and $\Delta n = 2$ are allowed.

A.   Gapped bilayer graphene

Graphene and bilayer graphene effect the transmission and the Faraday rotation in a linear order in the fine structure constant whereas the reflected light intensity is quadratic in α. Therefore, let us discuss the characteristics of the transmitted light through bilayer
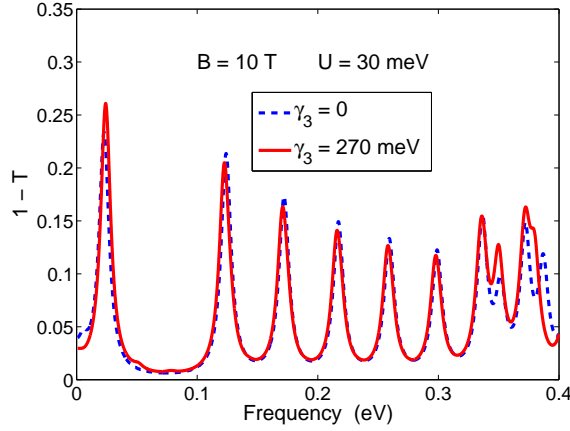
Figure 9: (Color online) Transmission spectra of gapped bilayer graphene without and with trigonal warping (dashed and solid lines, correspondingly) at 10 T and $U = 30$ meV; the band parameters used are $v = 1 \times 10^8$ cm/s, $\gamma_1 = 360$ meV, $\gamma_4 = -150$ meV, $\varepsilon_F = 30$ meV, others are listed in Fig. The relaxation frequency is supposed as $\Gamma = 5$ meV.

graphene where the effects have a maximum value. For this case, Eq. (38) is valid without the integration over the z momentum component. The conductivity units should be taken now as $\sigma_0 = e^2/4\hbar$. In the approximation linear in conductivities, the transmission coefficient T and the Faraday angle for the free standing bilayer write as

$$1 - T = \frac{4\pi}{c}\mathrm{Re}\,\sigma_{xx}, \Theta_F = \frac{2\pi}{c}\mathrm{Re}\,\sigma_{xy}\,. \tag{39}$$

Results of calculations are shown in Figs. 9 and 10. The peaks in absorption, Fig. 9 correspond to the electron transitions. There is the series of seven lines in the 0.1–0.4 eV interval. They are doublets excited by the electron transitions of the type $|2n\rangle \to |3, n+1\rangle$ and $|3n\rangle \to |2, n+1\rangle$ for n from 2 to 8. Two weaker lines at 350 and 380 meV are resulted from the $|10\rangle \to |31\rangle$ and $|21\rangle \to |42\rangle$ transitions, correspondingly. There is strongest line at 24 meV excited by the $|21\rangle \to |32\rangle$ transition. All these lines obey the selection rule $\Delta n = 1$.

The very weak lines at 51 and 78 meV owe their appearance to the $\Delta n = 2$ transitions $|21\rangle \to |33\rangle$ and $|10\rangle \to |22\rangle$.

In general, the effect of the small constants γ_3 and γ_4 is seen more on the low levels $|10\rangle$ and $|21\rangle$.
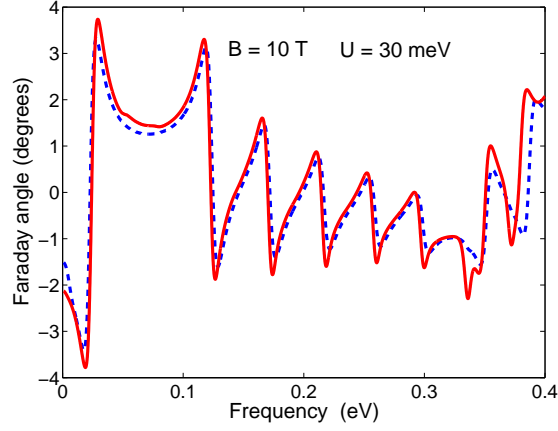
21

Figure 10: (Color online) Faraday rotation in gapped bilayer graphene; parameters used are the same as in Fig. 9.
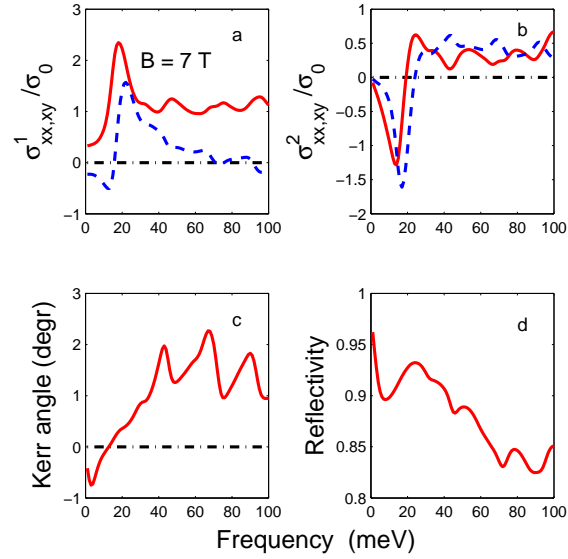

Figure 11: (Color online) Real (a) and imaginary (b) parts of the longitudinal (xx, solid line) and Hall (xy, dashed line) dynamical conductivities calculated for one graphite layer in units of $\sigma_0 = e^e/4\hbar$; Kerr angle (c) and reflectivity (d). The magnetic field $B = 7$ T, the temperature T = 0.1 meV is less than the level broadening $\Gamma = 3.5$ meV.

The transition frequencies in the Faraday rotation, Fig. 9 are determined by the derivative maximum values.
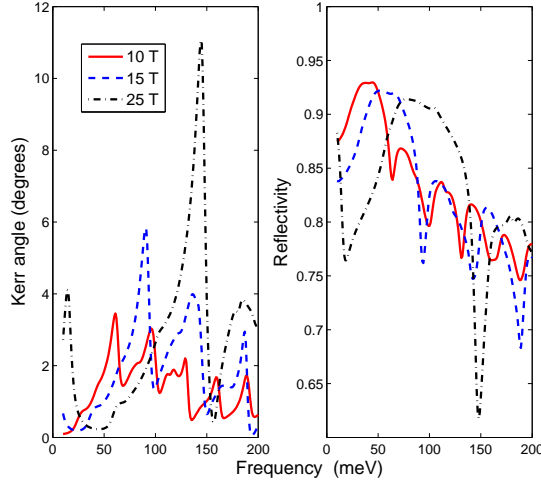
Figure 12: (Color online) Kerr angle and reflectivity at 10, 15, and 25 T.

B. Graphite

Using the conductivities Eqs. (38), one finds the complex bulk dielectric function $\varepsilon_{ij} = \delta_{ij} + 4\pi i \sigma_{ij}/\omega$ and the reflection coefficient and the Kerr rotation (see, e.g.,[61])

$$R = \frac{1}{2}(|r_+|^2 + |r_-|^2), \Theta_K = \frac{1}{2}\arg(r_- r_+^*),$$

where $r_\pm = (1 - \sqrt{\varepsilon_\pm})/(1 + \sqrt{\varepsilon_\pm})$ are the reflection Fresnel coefficients for two circular polarizations with $\varepsilon_\pm = \varepsilon_{xx} \pm \varepsilon_{xy}$.

The parameters of Eq. (2) used in the calculations are listed in Table I (see also Ref.[62]). The hopping integrals γ_0 to γ_3 are close to the values determined in observations of the semiclassical ShdH effect. The Fermi energy equal to $\varepsilon_F = -4.1$ meV agrees at the zero magnetic field with the measurements of the extremal Fermi-surface cross sections and the masses of holes and electrons. Connections with the notation for similar parameters of the SWMC model are given in the "SWMC" line. The values of parameters γ_4, γ_5, and Δ determined in various experiments are very different; we use γ_5 and Δ obtained by Doezema et al[4] (given in Table I in the "SWMC" notations) and take the approaching value for γ_4. In the quantum limit, when electrons and holes occupy only $|10\rangle$ and $|21\rangle$ levels, the Fermi energy must cross these close levels at the middle of the KH line. It means that the Fermi level becomes higher at such the magnetic fields taking the value $\varepsilon_F \approx -1$ meV.

The results of calculations are represented in Figs. 11-12. Let us emphasize that the

imaginary part of the dynamical conductivity is of the order of the real part.

One can see in Fig. 11 (a), that the averaged longitudinal conductivity calculated per one graphite layer tends to the graphene universal conductance. The main contribution in the sharp 16-meV line is resulted from the electron $|21\rangle \to |32\rangle$ transition (15 meV) about the K point (see Fig. 4) where the $|32\rangle$ level coincides with the Fermi level (within an accuracy of the width Γ or temperature T). Then, the transitions $|22\rangle \to |21\rangle$ produce the broad band. The low-frequency side of the band (23 meV, at the intersection of the $|21\rangle$ level with the Fermi level) contributes into the 16-meV line. In the same 16-meV line, the transitions $|32\rangle \to |33\rangle$ can contribute as well if the band $|32\rangle$ contains the electrons.

The next doublet at 43 meV arises from the transitions $|23\rangle \to |32\rangle$ and $|22\rangle \to |33\rangle$ at the K point. The 68- meV doublet appears as the splitting of the $|24\rangle \to |33\rangle$ (65 meV) and $|23\rangle \to |34\rangle$ (69 meV) transitions due to the electron-hole asymmetry at the K point of the Brillouin zone.

The 89-meV line is more complicated. First, there are the electron transitions $|24\rangle \to |35\rangle$ (89 veV) and $|25\rangle \to |34\rangle$ (90 meV) near the K point. Besides, the transitions $|11\rangle \to |10\rangle$ (95 meV) near the H point make a contribution as well. All these lines obeying the selection rule $\Delta n = 1$ are strong. There are two weak lines in the frequency range. One ($|24\rangle \to |32\rangle$) is seen at 55 meV as a shoulder on the theoretical curve. Another, at 31 meV, results from the transitions $|10\rangle \to |32\rangle$ near the K point.

The positions of the lines for fields in the range of $10 - 30$ T agree with observations of Refs.[8,18].

The optical Hall conductivity $\sigma_{xy}(\omega)$ in the ac regime is shown in Figs. 11 (a) and 11 (b). The conductivities $\sigma_{xx}(\omega)$ and $\sigma_{xy}(\omega)$ allow calculating the Kerr rotation and the reflectivity as functions of frequency [see Figs. 11 (c) and 11 (d)]. It is evident that the interpretation of the Kerr rotation governed by the conductivity $\sigma_{xy}(\omega)$ is much more complicated in comparison with the longitudinal conductivity. The Kerr angle and reflectivity shown in Fig. 12 for the different magnetic fields demonstrate the strong field dependence of the magneto-optic phenomena.

VII.   SUMMARY AND CONCLUSIONS

In conclusions, we have evaluated the perturbation theory for the matrix Hamiltonian, which permits to calculate the corrections to eigenvalues resulting from the small matrix elements particularly from the trigonal warping. The trigonal warping in graphite can be considered within the perturbation theory at strong magnetic fields larger than 1 T approximately. For weak magnetic fields, when the Fermi energy much larger than the cyclotron frequency, the semiclassical quantization with the Berry phase included can be applied. We have found that the main electron transitions obey the selection rule $\Delta n = 1$ for the Landau number n, however the $\Delta n = 2$ transitions due to the trigonal warping with the small probability are also essential. In graphite, the electron transitions at the K, H points as well as at intersections of the Landau levels with the Fermi level make contributions into conductivity. The good agreement between the calculations and the measured Kerr rotation and reflectivity in graphite in the quantizing magnetic fields is achieved. The SWMC parameters are used in the fit taking their values from the previous dHvA measurements and increasing the Fermi energy value for the case of the strong magnetic fields.

---

[1] J.C. Slonchewski and P.R. Weiss, Phys. Rev. **109**, 272 (1958); J.W. McClure, Phys. Rev. **108**, 612 (1957).

[2] H. Suematsu, S-i. Tanuma, J. Phys. Soc. Japan, **33**, 1619 (1972).

[3] W.W. Toy, M.S. Dresselhaus, G. Dresselhaus, Phys. Rev. B **15**, 4077 (1977).

[4] R.E. Doezema, W.R. Datars, H. Schaber, A. Van Schyndel, Phys. Rev. B **19**, 4224 (1979).

[5] E. Mendez, A. Misu, M.S Dresselhaus, Phys. Rev. B **21**, 827 (1980).

[6] Z.Q. Li, S.-W. Tsai, W.J. Padilla, S.V. Dordevic, K.S. Burch, Y.J. Wang, D.N. Basov, Phys. Rev. B **74**, 195404 (2006).

[7] M. Orlita, C. Faugeras, G. Martinez, D.K. Maude, M.L. Sadowski, M. Potemski, Phys. Rev. Lett. **100**, 136403 (2008).

[8] M. Orlita, C. Faugeras, J.M. Schneider, G. Martinez, D.K. Maude, M. Potemski, Phys. Rev. Lett. **102**, 166401 (2009).

[9] M. Orlita, M. Potemski, Semicond. Sci. Technol. **25**, 063001 (2010).

[10] I. Crassee, J. Levallois, A. L. Walter, M. Ostler, A. Bostwick, E. Rotenberg, T. Seyler, D. van der Marel, A. Kuzmenko, Nature Physics **7**, 48 (2011).

[11] Y. Kopelevich, J.H.S. Torres, R.R. da Silva, F. Mrowka, H. Kempa, P. Esquinazi, Phys. Rev. Lett. **90**, 156402 (2003).

[12] I. A. Luk'yanchuk, Y. Kopelevich, Phys. Rev. Lett. **97**, 256801 (2006).

[13] Z. Jiang, Y. Zhang, H.L. Stormer, P. Kim, Phys. Rev. Lett. **99**, 106802 (2007).

[14] J.M. Schneider, M. Orlita, M. Potemski, D.K. Maude, Phys. Rev. Lett. **102**, 166403 (2009).

[15] A.N. Ramanayaka, R. G. Mani, Phys. Rev. B **82**, 165327 (2010).

[16] L.A. Falkovsky Phys. Rev. B **84**, 115414 (2011).

[17] G. Li, E.Y. Andrei, Nature Phys. **3**, 623 (2007).

[18] K.-C. Chuang, A.M.R. Baker, R.J. Nicholas, Phys. Rev. B **80**, 161410(R) (2009).

[19] L.M. Zhang, Z.Q. Li, D.N. Basov, M.M. Fogler, Z. Hao, M.C. Martin, Phys. Rev. B **78**, 235408 (2008).

[20] H. Ushio, T. Uda, Y. Uemura, J. Phys. Soc. Japan, **33**, 1551 (1972).

[21] K. Nakao, J. Phys. Soc. Japan, **40**, 761 (1976).

[22] B.Partoens and F.M. Peeters, Phys. Rev. B **74**, 075404 (2006).

[23] A. Grüneis, C. Attaccalite, L. Wirtz, H. Shiozawa, R. Saito, T. Pichler, A. Rubio, Phys. Rev. B **78**, 205425 (2008).

[24] A.B. Kuzmenko, I. Crassee, D. van der Marel, P. Blake, K.S. Novoselov, Phys. Rev. B **80**, 165406 (2009).

[25] L.A. Falkovsky, Zh. Eksp. Teor. Fiz. **49**, 609 (1965) [Sov. Phys. JETP **22**, 423 (1966)].

[26] G. Dresselhaus, Phys. Rev. B **10**, 3602 (1974).

[27] D.C. Elias, R.V. Gorbachev, A.S. Mayorov, S.V. Morozov, A.A. Zhukov, P. Blake, L.A. Ponomarenko, I.V. Grigorieva, K.S. Novoselov, F. Guinea, A.K. Geim, Nat. Phys. **7**, 701 (2011).

[28] A.A. Abrikosov and S.D. Beneslavsky, Sov. Phys. JETP **32**, 699 (1971).

[29] J. Gonzalez, F. Guinea and M.A.H. Vozmediano, Nucl. Phys. B **424**, 595 (1994); J. Gonzalez,

F. Guinea and M.A.H. Vozmediano, Phys. Rev B **59**, 2474 (1999).

[30] E.G. Mishchenko, Phys. Rev. Letts. **98**, 216801 (2007).

[31] E. McCann, V.I. Fal'ko, Phys. Rev. Lett. **96**, 086805 (2006).

[32] C.L. Lu, C.P. Chang, Y.C. Huang, R.B. Chen, and M.L. Lin, Phys. Rev. B **73**, 144427 (2006).

[33] T. Ohta, A. Bostwick, T. Seyller, K. Horn, and E. Rotenberg, Science **313**, 951 (2006).

[34] L.M. Zhang, Z.Q. Li, D.N. Basov, M.M. Foger, Z. Hao, and M.C. Martin, Phys. Rev. B **78**, 235408 (2008).

[35] A.B. Kuzmenko, E. van Heumen, D. van der Marel, P. Lerch, P. Blake, K.S. Novoselov, A.K. Geim, Phys. Rev. B **79**, 115441 (2009).

[36] Z.Q. Li, E.A. Henriksen, Z. Jiang, Z. Hao, M.C. Martin, P. Kim, H.L. Stormer, and D.N. Basov, Phys. Rev. Lett. **102**, 037403 (2009).

[37] E.V. Castro, K.S. Novoselov. S.V. Morozov, N.M.R. Peres, J.M.B. Lopes dos Santos, Johan Nilsson, F. Guinea, A.K. Geim, and A.H. Castro Neto, Phys. Rev. Lett. **99**, 216802 (2007).

[38] E.J. Nicol, J.P. Carbotte, Phys. Rev. B **77**, 155409 (2008).

[39] K.F. Mak, C.H. Lui, J. Shan, and T.F. Heinz, Phys. Rev. Lett. **102**, 256405 (2009).

[40] A.B. Kuzmenko, I. Crassee, D. van der Marel, P. Blak, and K.S. Novoselov, arXiv:0908.0672 (2009).

[41] P. Gava, M. Lazzeri, A.M. Saitta, and F. Mauri, Phys. Rev. B **79**, 165431 (2009).

[42] J.C. Charlier, X. Gonze, and J.P. Michenaud, Phys.Rev. B **43**, 4579 (1982).

[43] L.A. Falkovsky and A.A. Varlamov, cond-mat/0606800, Eur. Phys. J. B **56**, 281 (2007).

[44] V.P. Gusynin, S.G. Sharapov, and J.P.Carbotte, Phys. Rev. **B 75**, 165407 (2007); cond-mat/0607727, Phys. Rev. Lett. **96**, 256802 (2006).

[45] L.A. Falkovsky, Phys. Rev. B **75**, 033409 (2007).

[46] L.A. Falkovsky, S.S. Pershoguba, Phys. Rev. B **76**, 153410 (2007).

[47] R.R. Nair, P. Blake, A.N. Grigorenko, K.S. Novoselov, T.J. Booth, T. Stauber, N.M.R. Peres, A.K. Geim, Science **320**, 5881 (2008).

[48] Z.Q. Li, E.A. Henriksen, Z. Jiang, Z. Hao, M.C. Martin, P. Kim, H.L. Stormer, D.N. Basov, Nature Physics **4**, 532 (2008).

[49] K.F. Mak, M.Y. Sfeir, Y. Wu, C.H. Lui, J.A. Misewich, and Tony F. Heinz, Phys. Rev. Lett. **101**, 196405 (2008).

[50] A.B. Kuzmenko, E. van Heumen, F. Carbote, D. van der Marel, Phys. Rev. Lett. **100**, 117401

(2008).

[51] L.A. Falkovsky, Phys. Rev. B **82**, 073103 (2010).

[52] M.V. Berry, Proc. Roy. Soc. London, Ser. A **392**, 45 (1984).

[53] G.P. Mikitik, Yu.V. Sharlai, Zh. Eksp. Teor. Fiz. **114**, 1357 (1998)[Sov. Phys. JETP **87**, 747 (1998)]; Phys. Rev. B **67**, 115114 (2003).

[54] P. Carmier, D. Ullmo, Phys. Rev. B **77**, 245413 (2008).

[55] A.A. Taskin, Y. Ando, Phys. Rev. B **84**, 035301 (20011).

[56] E.V. Kurganova, H.J. van Eleferen, A. McCollam, L.A. Ponomarenko, K.S. Novoselov, A. Veligura, B.J. van Wees, J.C. Maan, U. Zeitler, Phys. Rev. B **84**, 121407 (20011).

[57] Cheol-Hwan Park, N. Marzari, Phys. Rev. B **84**, 205440 (2011).

[58] Singhun Park, H.-S. Sim, Phys. Rev. B **84**, 235432 (2011).

[59] Y. Liu, G. Bian, T. Miller, T.-C. Chiang, Phys. Rev. Lett. **107**, 166803 (2011).

[60] L.M. Zhang, M.M. Fogel, D.P. Arovas, Phys. Rev. B **84**, 075451 (2011).

[61] J. Levallois, M. Tran, and A.B. Kuzmenko, arXiv:1110/2754v2.

[62] N.B. Brandt, S.M. Chudinov, Ya.G. Ponomarev, *Semimetals I. Graphite and its compaunds* (Elsevier, Amsterdam, 1988).